Case Studies in Thermal Engineering 55 (2024) 104156

Contents lists available at ScienceDirect

Case Studies in Thermal Engineering

journal homepage: www.elsevier.com/locate/csite

Fire retardation, compressive strength and durability analysis of concrete reinforced with novel plasters: An experimental, computational and statistical research

Ilker Ustabas [a], Pinar Mert Cuce [b], Emre Alvur [c], Duygu Kesepara [a], Yusuf Nadir Yilmaz [c], Erdem Cuce [c, d, *], Saad Alshahrani [e, f]

[a] Department of Civil Engineering, Faculty of Engineering and Architecture, Recep Tayyip Erdogan University, Zihni Derin Campus, 53100, Rize, Turkey
[b] Department of Architecture, Faculty of Engineering and Architecture, Recep Tayyip Erdogan University, Zihni Derin Campus, 53100, Rize, Turkey
[c] Department of Mechanical Engineering, Faculty of Engineering and Architecture, Recep Tayyip Erdogan University, Zihni Derin Campus, 53100, Rize, Turkey
[d] School of Engineering and the Built Environment, Birmingham City University, B4 7XG, Birmingham, UK
[e] Department of Mechanical Engineering, College of Engineering, King Khalid University, P.O. Box 394, Abha, 61421, Saudi Arabia
[f] Centre for Engineering and Technology Innovations, King Khalid University, Abha, 61421, Saudi Arabia

GRAPHICAL ABSTRACT

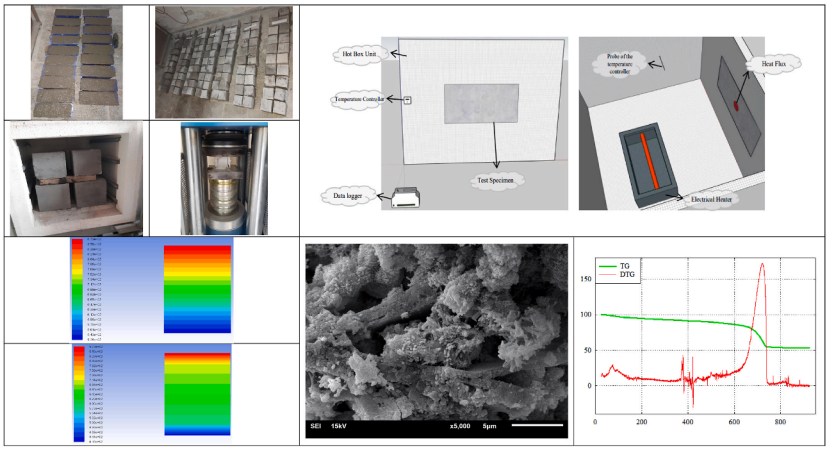

* Corresponding author. Department of Mechanical Engineering, Faculty of Engineering and Architecture, Recep Tayyip Erdogan University, Zihni Derin Campus, 53100, Rize, Turkey.
E-mail address: erdem.cuce@erdogan.edu.tr (E. Cuce).

https://doi.org/10.1016/j.csite.2024.104156
Received 4 December 2023; Received in revised form 7 February 2024; Accepted 18 February 2024
Available online 24 February 2024

ARTICLE INFO

Keywords:
Fire retardation
Contemporary insulation plaster
Thermal resistance
Mechanical degradation
Compressive strength
Durability

ABSTRACT

Concrete is an essential component of the construction industry, valued for its high compressive strength (CS) and durability. However, when exposed to extreme conditions like fire without protective structural elements, its physical integrity deteriorates rapidly, leading to significant alterations in its mechanical properties. This research aims to provide a potential solution to this issue by assessing the fire resistance of various concrete samples, including unplastered (UNP), roughly plastered (RP), and those with contemporary insulation plaster (CIP) substitutions, at different thicknesses. These samples are subjected to varying temperatures and exposure times within an oven, followed by CS testing. These temperature levels and time intervals correspond to 300 °C, 450 °C, and 600 °C, with the time range is restricted to 60, 90, and 120-min, respectively. The results indicate that an increase in sample thickness correlates with a reduction in concrete degradation at high temperatures. Moreover, the findings reveal that after 120-min of exposure at 600 °C, UNP, RP, and CIP-reinforced samples achieve CSs of 27.435 MPa, 27.74 MPa, and 30.28 MPa, respectively. Notably, the 3 cm CIP-reinforced sample exhibits a CS exceeding 30 MPa under the most extreme conditions. The research incorporates regression and computational fluid dynamics (CFD) analyses to complement the experimental investigation. The regression analysis suggests that CIP-reinforced samples can withstand temperatures up to 600 °C for approximately 173-min, while the study implies that they could endure temperatures as high as 861 °C during a 120-min exposure.

Nomenclature

Descriptions of symbols (Units)

ρ	Density (kg/m^3)
k	Thermal conductivity (W/mK)
U	Total heat transfer coefficient (W/m^{2}K)
F_{CS}	Compressive strength force (MPa)
t_{exp}	Exposure time (min)
T	Temperature (°C)

Abbreviations

CIP	Contemporary insulation plaster
UNP	Unplastered
RP	Rough plaster
GP	Gypsum perlite
GMW	Gypsum mineral wool
CS	Compressive strength
EP	Expended perlite
GGBFS	Ground granulated blast furnace slag
AS	Alluvial sand
CCB	Crushed basalt
CCG	Crushed gneiss
NS	River sand
CRS	Crushed sand
CA	Crushed coarse aggregate

1. Introduction

The elevated temperatures that occur after the fire not only affect people but also directly influence the construction elements in the buildings adversely [1]. Concrete, which has a vital place among building materials, can exchange its physical and chemical structures against very high temperatures that occur in fires [2–7], as well as prevent environmental hazards [8]. These deteriorations begin when it reaches approximately 400 °C. The first corruption occurs in the hardened cement paste. Afterwards, with the temperature reaching about 900 °C, the decomposition continues severely with the complete disappearance of the calcium-silicate-hydrate gel [9]. As a result of this extreme situation, the concrete structure gradually or very rapidly distorts depending on the situation, along with severe decreases in strength and durability [10]. It is of vital significance for the concretes, which are frequently encountered in buildings, to withstand high temperatures for up to 2-h, which is suitable for the evacuation of people during a fire. During this period, studies aimed at minimising the degradation in the structure should become a necessity rather than a choice because it is unde-

niable that the building is in danger of collapsing as a result of a minor worsening during the fire [11]. Even though the temperature and severity of the fire vary in accordance with the substances in the environment, extremely high temperatures such as 1000 °C usually take place. It is so valuable to redound the strength of building elements, for instance concrete, which is one of the methods of diminishing the loss of life and property that may happen due to these elevated temperatures. Considering the structure of the concrete, researchers show that if the concrete is exposed to high temperatures, internal breakdown can quickly begin, and collapses can be formed [12]. That's why researchers are currently engaged in ongoing research on fire retardation, striving to discover a viable solution.

Apart from employing steel, polymer, perlite, basalt, and carbon-derived fibres, as mentioned in various studies in the literature for enhancing fire resistance, currently, researchers are actively investigating the potential of insulation plasters with the aim of achieving the same objective. In a study by Kiran et al. [12], it is heated by a temperature-controlled oven at 821 °C for 30-min, 925 °C for 60-min, and 986 °C for 90-min on samples coated with sand plaster, which is known as traditional plaster, gypsum perlite (GP) plaster and gypsum mineral wool (GMW) plaster. As a result, a more successful outcome is obtained in the pressure tests performed after the GMW and GP plaster-coated samples are suffered from high temperatures compared to the traditional plaster-coated sample. The study is carried out to explain that by using fibres such as polypropylene, nylon and steel in the preparation stage of concrete, in the case of a possible fire, a better resistance against the fire will be obtained if these fibres are used in what proportion by Lee et al. [13]. According to the test results, the best resistance to elevated temperatures during a fire will be achieved if the fibres are 0.2% for polypropylene, 0.2% for nylon, and 0.5% for steel by volume. Asamatdinov et al. [14] investigate the effect of clay-gypsum-based modified binder utilised as the main component of plasters at elevated temperatures such as fire. As a result of the tests, it is revealed that after a 20% increase in the bending strength of the sample, the plaster coating on the piece is the more resistant against the temperature and, hence, the more effective method at very high temperatures. Li et al. [15] are pioneered a study researching the efficacy of the samples under variable temperatures of 200-400-600-800 °C with a non-combustible coating as well as the influence of cooling with air and water. According to the results obtained from the samples subjected to the temperatures specified in the study, it is recorded that the CS of the examples is about 10.4 %–93.1%. At the same time, the results indicate that after the samples suffer from quite high temperatures (800 °C), in the event of cooling with water, a decrease of nearly 43.5% is observed in the CS of the sample. Aydın and Baradan [16] explore the behaviour of concrete examples containing 0, 20, 40 and 60% pumice and fly ash at high temperatures. Temperatures are set at 300, 600, and 900 °C and exposed at these temperatures for 3-h. In addition, the samples are held in two types of cooling: water and air, and the alterations in their internal structures are monitored. In light of the information obtained from the examinations, it is understood that the sample containing 60% fly ash successfully survived the highest temperature condition has been recorded. Kiran et al. [17] conduct a study in which they compare their actions against extremely high temperatures by coating the Clay Brick Wall with various mortars, including M-sand, vermiculite, and perlite mortars. The variables determined in the study are temperature and time, designated as 30-min at 821 °C, 60-min at 925 °C, 90-min at 986 °C, and 120-min at 1029 °C, respectively. As a result of the tests, it is figured out that the sample covered with perlite mortar provides better fire protection under all conditions. Zulkifeli and Saman [18] try to improve a sand mortar with expanded perlite (EP) aggregate variability of 0, 10, 20, 30, and 40% by volume. The temperature variables in the study are stated as room temperature, 200, 400, 700, and 1000 °C, separately, and the CS test is acted on the samples at these temperatures. As a result of the study, whilst the EP aggregate of 0% shows the best CS between room temperature and 400 °C, the sample with EP aggregate of 20% at elevated temperatures between 700 and 1000 °C indicates the best resistance. In one of the studies of Aydın [19], he examines the effects of samples of cement-based pumice mortars containing dissimilar quantities of ground granulated blast furnace slag (GGBFS) under temperatures reaching a maximum of 900 °C. As a result of the findings, with 80% GGBFS, mitigation between 23% and 28% at room temperature compared to the same sample at 900 °C of the plaster is seen in the CS test. Nevertheless, this decrease is up to 70% in the instance that does not have GGBFS. Moreover, the CS of 40% GGBFS in slow cooling at 900 °C has the highest value as 18 MPa, however, the ratios of temperature differences in the findings show that with the increase in GGBFS ratio, the resistance to high temperatures increases proportionally and therefore leads better resistance. Koksal et al. [20] identify 3, 4, 5, and 6 ratios dissimilar types of samples with expanded vermiculite powder divided by cement proportions. These samples are heated to 20, 300, 600, 900, and 1100 °C temperatures, and CS test is applied at the end of the processes. Upon the completion of the test, it is noted that the CS of the sample with a mixing ratio of 4 is decent at elevated temperatures. Ma et al. [21] manage a study in which they covered concrete samples with 0, 5, 10, and 20% volumes of aerogel and exposed them to temperatures of 200, 400, 600, 800, and 1000 °C, determined as variables. As an example from the working data, mitigation of 1%–25.9% is observed between the temperatures of 200°C–600 °C of the 10% volume aerogel-coated sample compared to its initial value. In comparison, a 4.7–32.2% diminishment is influenced at temperatures between 800°C and 1000 °C. Li et al. [22] analyse the CS of C40, C60, and C70 series concretes at five dissimilar temperatures, from 200 °C to 1000 °C, increasing 200 °C each time. The type of furnace used to reach these temperatures is determined as an oil furnace. A fire that will come about in the real condition takes place suddenly and raises the temperature abruptly. Therefore, it is preferred because the temperature rises suddenly in this furnace. In accordance with the test, C70 delivers the highest CS at each specified temperature. Meanwhile, among the samples at 600 °C, it is observed that the C70 type sample has a more pronounced higher CS than the others. In addition, following the information obtained at the end of the tests, the increment in the sample size proportionally reveals a profound effect on the compression resistance. In a study by Bilow and Kamara [23], concrete samples having siliceous aggregate are tested at elevated temperatures. According to the information obtained as a result of this test, they point out that whilst it does not have a remarkable variation in the strength of concrete up to 400 °C, there is a gradual change at 650 °C and beyond, and there is a loss of 55% in the CS test. Alaskar et al. [24] pursue a study aiming to experimentally test its effectiveness by substituting basalt fibre in concrete to delay the deterioration of the structure of concrete at high temperatures. In this study, basalt fibre is added at dosages of 0.25%, 0.5%, 0.75% and 1% during the preparation phase of the concrete samples, and these samples are kept in an oven at 600 °C. According to

the test result, the remaining strengths for the concrete samples containing varying percentages of basalt fibres (0%, 0.25%, 0.50%, 0.75%, and 1%) are measured at 28.4%, 30.5%, 30.7%, 28.9%, and 34.3% respectively. Reddy and Ramaswamy [25] manage an experiment in which they subject 28-day and 365-day concrete samples, containing granite aggregate and iron ore in the aggregate and utilising both pure cement and fly ash-substituted cement to various levels of stress within a furnace. The temperature inside the furnace is increased at a rate of 12 °C/min, reaching temperatures of 200 °C, 374 °C, 500 °C, 700 °C, and 800 °C. The concrete samples, with a water/cement ratio of 0.4 and a cement density of 385 kg/m^3, are assessed for CS after exposure to these elevated temperatures. The results observe that, compared to concrete samples kept at room temperature, the CS of the concretes exposed to high temperatures experience approximately a 3% reduction at 200 °C, a 20% mitigation at 374 °C, and a 40% diminishment at 500 °C. This minimisation in CS become more significant as the temperature increased, with a 55% decline at 700 °C and a substantial 75% lessening at 800 °C. Furthermore, during the examination of concrete manufactured using cements that include 40% fly ash, it is seen that the reduction in CS at 800 °C reaches as high as 80%. In their study, Molay et al. [26] investigate the changes in CS of concrete batches made from three different types of forms: alluvial sand from the Sanaga River (AS), crushed basalt (CCB), and crushed gneiss (CCG). These concretes have a water/cement ratio of 0.47 and are subjected to temperatures of 300, 600, and 900 °C. The researchers measure the CS of the samples at the desired temperature level. After reaching the specified temperatures, each sample is suffered from air and gradually cooled at a rate of 4 °C per minute. The experimental results show that there is an increment in CS for specimens at 300 °C. Specifically, the increase is measured as 5% for AS, 6% for CCB, and 4% for CCG. However, at 600 °C, depending on the type of aggregate used, there is a significant decrease in CS ranging from 10% to 35%. This reduction becomes even more pronounced at 900 °C, with an average decrease of 74%. Consequently, the samples made from AS and CCG sands are found to exhibit the highest resistance to high temperatures. In the study by Shen and Xu [27] examines how the moisture content and voids within concrete impact its CS when exposed to high temperatures. They prepare the concrete by adding 380 kg of cement and 190 kg of water for one cubic meter of concrete. This ensures that the concrete is fully saturated with water. The concrete samples are then subjected to various temperatures, specifically 20 °C, 40 °C, 105 °C, 150 °C, 200 °C, and 250 °C, until the vacuum level attains 0.3–0.4 torr. Subsequently, the researchers quantify the CS of the concrete. Compared to the CS of 100% saturated concrete at 20 °C, the concrete samples heated to 40 °C and reduced to 0% humidity exhibit a 10% increase in CS. Likewise, concrete samples with 0% humidity at 105 °C show a remarkable 55% increment in CS when compared to fully saturated concrete at 20 °C. However, while the temperature is raised to 200 °C, there is a diminishment in CS, ranging from 9% to 20%, depending on the moisture content of the concrete, in comparison to the CS of fully saturated concrete at 20 °C. This decrease becomes even more significant at 250 °C, with reductions ranging from 19% to 30% in concrete samples with varying moisture content, again compared to the CS of fully saturated concrete at 20 °C. In their investigation, Mundhada and Pofale [28] disclose alterations in the CS of concrete specimens on suffered from elevated temperatures. The study encompasses a total of 90 samples, shaped as 150 mm cubes. These samples, categorised into three distinct mixture designs (M30, M25, and M20), consist of 30 specimens each. The experimental conditions involve temperatures of 200 °C and 800 °C, with corresponding durations of 1-h and 2-h. Subsequent to exposure to high temperatures, the samples are allowed to rest outdoors for 24-h. The findings indicate that, generally, concrete specimens exhibit minimal damage up to 500 °C and can be effectively restored for further use. However, severe impairment becomes evident in samples subjected to temperatures of 650 °C and beyond, rendering them irreparable. Sancak et al. [29] investigate the CS and weight variations in lightweight concrete incorporating pumice in comparison to conventional aggregate concrete. The experimental conditions involve 20, 100, 400, 800, and 1000 °C temperatures. The samples are prepared with varying proportions of silica fume (0%, 5%, and 10% as a replacement for cement) and include 2% superplasticiser material. The findings reveal that, despite both lightweight concrete and standard concrete experiencing similar physical deteriorations, lightweight concrete demonstrates superior strength as temperatures increase. For instance, at 800 °C, lightweight concrete exhibits 28% protection against degradation, whilst standard concrete observes 16%. Notably, two samples display a loss of strength at 1000 °C.

Fire has critical perils in many senses, incredibly human, environmental and building elements. In the existing body of literature, numerous investigations have been conducted to increase the fire resistance of buildings. This study aims to test the effect of the CIP, which is different from other studies, on protecting the concrete block against high temperatures such as possible fire. In the study, 10 cm cubed concrete samples are coated with 1, 2, and 3 cm thick RP and CIP, as well as UNP samples are prepared. The samples are kept for 60, 90, and 120-min in an oven set at 300, 450, and 600 °C, and after these processes, each sample is subordinated to a CS test. Aside from the experimental test study, regression analysis and CFD simulation modelling are also investigated to demonstrate the significant efficacy of CIP in countering fire incidents. As a result, the aim of these experimental tests and analyses is to prove the effect of the CIP on the readers and to give a new perspective to the literature.

2. Methodology

Each surface of C30/37 class 10 cm cube concrete samples is covered with 1, 2, and 3 cm thick RP and CIP. Besides, sufficient samples for the test are left plain without any coating process. When the relevant articles in the literature are scanned, it shows that experimental studies are carried out by increasing the temperature to 900 °C in general and keeping the samples for 2–3 h in order to demonstrate the resistance of concrete against high temperatures. However, in this scope of the study, each sample is subjected to specified temperatures for durations of 60, 90, and 120-min after completing the coating process. These temperatures are set at 300, 450, and 600 °C within an oven. Afterwards, the current coatings on the samples retrieved from the furnace are stripped, and the samples undergo a CS test to measure and analyse their CS. The steps performed both prior to and following the experimental procedure are illustrated using images in Fig. 1.

Fig. 1. a. The concrete generated by pouring the prepped mortar into the mould, b. The phase where samples are being plastered, c. The situation in which samples are placed inside an oven and exposed to heat, d. The act of subjecting the samples to CS testing.

In Fig. 2, which illustrates the study's procedures, the initial step involves preparing samples in the form of 10 cm cubes to initiate experimental testing. Subsequently, these samples are coated with a specified plaster of a particular thickness to prepare them for testing. In the following stage, measurements of thermal conductivity (k-value) and total heat transfer coefficient (U-value) are taken using the hot box method, utilising one of the CIP samples. Once this phase is completed, each sample undergoes a CS test, with the

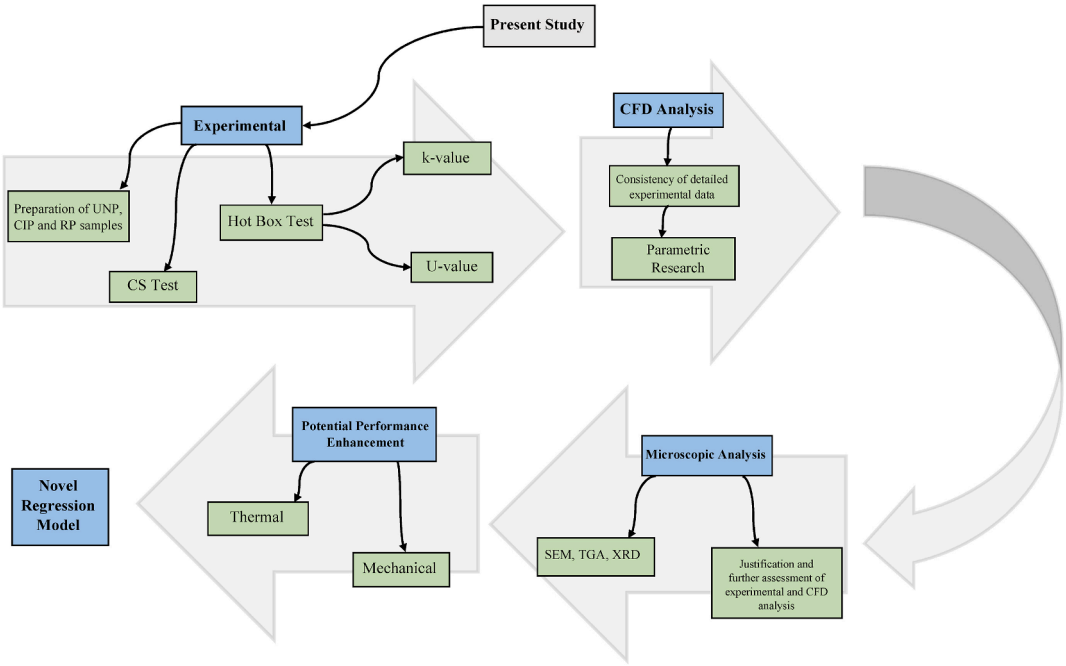

Fig. 2. The content and goal of the research.

recorded values noting any developments. Subsequent to these procedures, the internal structures of the samples are examined through microscopic analysis, confirming their relationship. Finally, for verification purposes, CFD analysis and regression modelling are employed. In summary, the study delves into the investigation of thermal and mechanical behaviours.

2.1. Contemporary insulation plaster

The CIP is manufactured following the guidelines of TSE EN 13501-1 standard and holds a certification of class A-1. It is formulated in adherence to global benchmarks for heat, water, and sound insulation, and it is particularly effective in providing crucial fire retardants. It exhibits the capability to endure temperatures of up to approximately 1000 °C for a duration of 3-h. Utterly devoid of carcinogenic elements, this plaster boasts an entirely natural composition and possesses breathable properties. Its composition is also engineered to hinder the development of issues like dampness, mould, and fungus that could manifest within structures. This study utilises the patented CIP, which marks the inaugural utilisation of boron mine resources in Turkey [30]. The details regarding the specifications of the CIP are provided in Table 1.

2.2. Aggregate granulometry and concrete

The line groups represented by green, red, and black in Fig. 3, denoted as A, B, and C, respectively, illustrate the thickness, ideal, and fineness limits per the TS 802 1985 standard. These limits are determined based on the granulometry curves of the mixture aggregate. Additionally, the aggregate represented by the granulometry curve shown in the blue curve symbolised as D consists of a blend of river sand (NS (0/4)), crushed sand (CRS (0/4)), and crushed coarse aggregate (CA (4/32)) in proportions of 20%, 35%, and 45% respectively.

The study utilises concrete of strength class C30/37 with a slump measurement of 18 cm. Table 2 displays the quantities of materials employed in 1 m^3 of concrete, along with the specific gravity and water absorption characteristics of the aggregates.

2.3. Hot box Unit

A co-heating test is conducted using a hot box to analyse the k-value of a sample within a controlled laboratory setting. The co-heating method, a dependable technique [31], is typically implemented in an unoccupied environment [32], enabling results to be

Table 1
Technical attributes of the CIP [30].

Fire Resistance	$A-1$
k-value	$0.13 W/mK$
CS	$CSII\ 2.448 N/mm^2$
Bond Strength	$0.50 N/mm^2$
Water Absorption	$W2\ 0.188 kg/m^2\ min^{0.5}$
Density (ρ)	$950 \pm 50 kg/m^3$
Sound Absorption	$15\ dB$

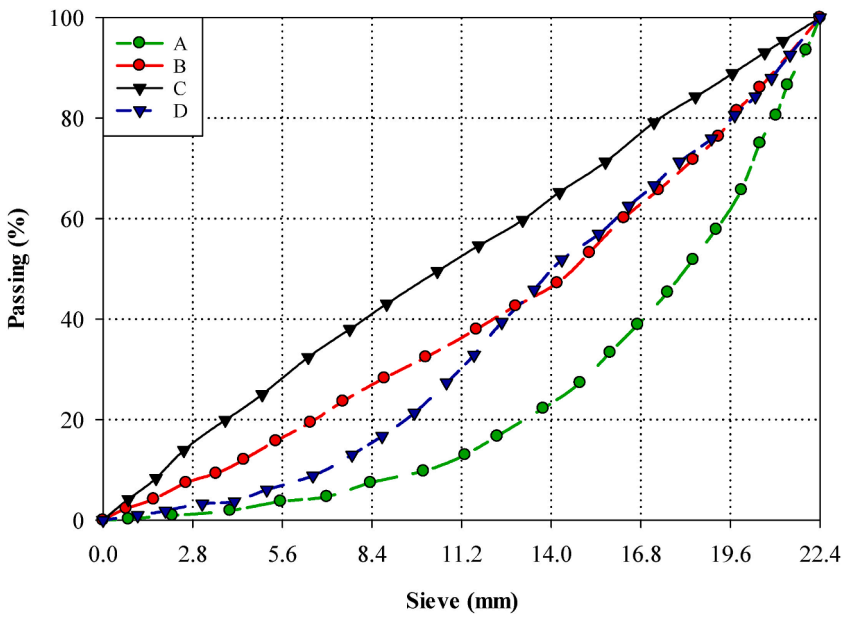

Fig. 3. Granulometry curve of aggregate utilised in concrete.

Table 2
Quantities of materials employed in the concrete mixture.

Material	Quantity (kg)	Specific Gravity	Water Absorption (%)
NS (0/4)	517	2.53	3.42
CRS (0/4)	505	2.47	5.68
CA (4/32)	757	2.78	2.06
Cement	396	3.1	
Water	178	1	
Chemical Additive	3.96	1.12	

obtained in an artificial setting with an indoor-outdoor temperature difference of at least 10 °C [33]. The laboratory-based experimental testing takes place in an adiabatic hot box, along with a surrounding section. Within the hot box, an electric heater is set to 25 °C through a temperature control unit. Additionally, the air conditioning system in the enclosed region ensures the required temperature difference, a crucial aspect of the test. T-type thermocouples are strategically positioned on the sample, with their readings connected to a data logger for recording temperature values. Furthermore, heat flux sensors are affixed to the sample surface within the system.

Fig. 4 provides a visual representation of the systems and their positions throughout the hot box experiment. Consequently, the resulting k-value is documented as 0.13 W/mK [30].

3. Results and discussion

The experimentation involves applying RP and CIP to each surface of C30/37 class 10 cm cube concrete samples. The thicknesses of the plaster coatings are varied: 0 cm (without coating), 1 cm, 2 cm, and 3 cm. Previous research endeavours have often involved experimental assessments of concrete strength under high temperatures, typically involving temperature elevation to 900 °C and holding samples for 2–3 h. Nevertheless, in this study, distinct temperatures are applied to each sample for durations of 60, 90, and 120-min following the conclusion of the coating procedure. Specifically, these temperatures are established as 300, 450, and 600 °C within an oven setting. Subsequently, the coatings currently present on the samples, which have been removed from the furnace, are stripped off. These samples then undergo a CS test, aimed at quantifying and analysing their CS.

Based on the outcomes illustrated in Fig. 5, as a result of the carried out tests, the CS of the C30/37 grade sample is determined to be around 43.9 MPa at room temperature. Moreover, upon analysing the CSs observed among the samples subjected to elevated temperatures, it is evident that the most substantial reduction occurs at 600 °C. For instance, in the case of the untreated sample at 600 °C, the recorded CSs for durations of 60, 90, and 120-min are noted as 40.23 MPa, 37.555 MPa, and 27.435 MPa, respectively. Particularly, there is a mitigation of 8.4%, 14.5%, and 37.5% for each value, respectively, when compared to the measurement taken at room temperature. Consequently, when the time is doubled for the samples, the reduction in CS increases by over fourfold. This emphasises that both the temperature and the duration of exposure play a substantial role in impacting the decrease in CS of concrete when subjected to high temperatures.

Fig. 6a displays CS data for various plaster thicknesses, including 0, 1, 2, and 3 cm. After exposing the specimens to different temperatures (room temperature, 300 °C, 450 °C, and 600 °C for 60, 90, and 120-min, these measurements are taken. Each set of columns in the graph represents the plaster thicknesses, with values on the y-axis indicating CS in MPa. In this scenario, it can be inferred that all three column blocks, with the exception of the room temperature block, pertain to a unified temperature. In that case, the temperature mentioned beneath each block should be understood as indicating an initial exposure time of 60-min, with the subsequent blocks representing 90 and 120-min until transitioning to the next temperature level. Furthermore, prior to conducting CS measurements, the specimens featuring conventional plaster and CIP undergo a treatment involving the removal of their plasters on the same day they suffer from elevated temperatures. Consequently, the chart illustrates how the CS changes for each plaster thickness under varying exposure conditions. For instance, in the case of plaster samples measuring 0, 1, 2, and 3 cm in

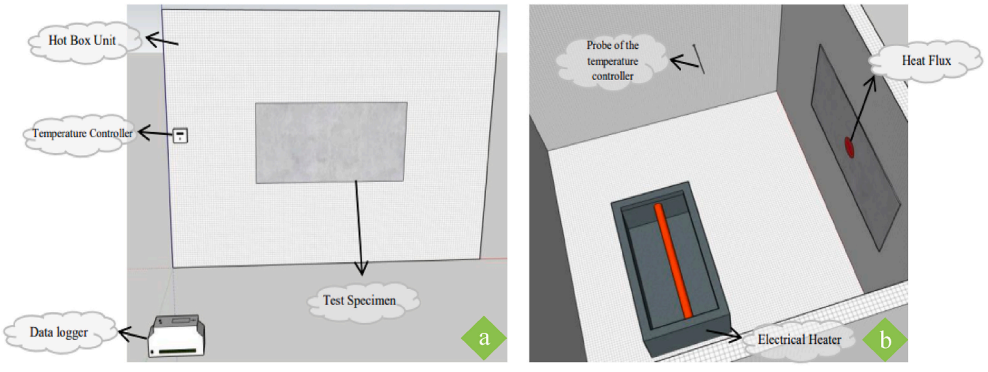

Fig. 4. a. An illustrative perspective of the test as observed from the external surroundings, b. A cutaway view of the interior of the hot box.

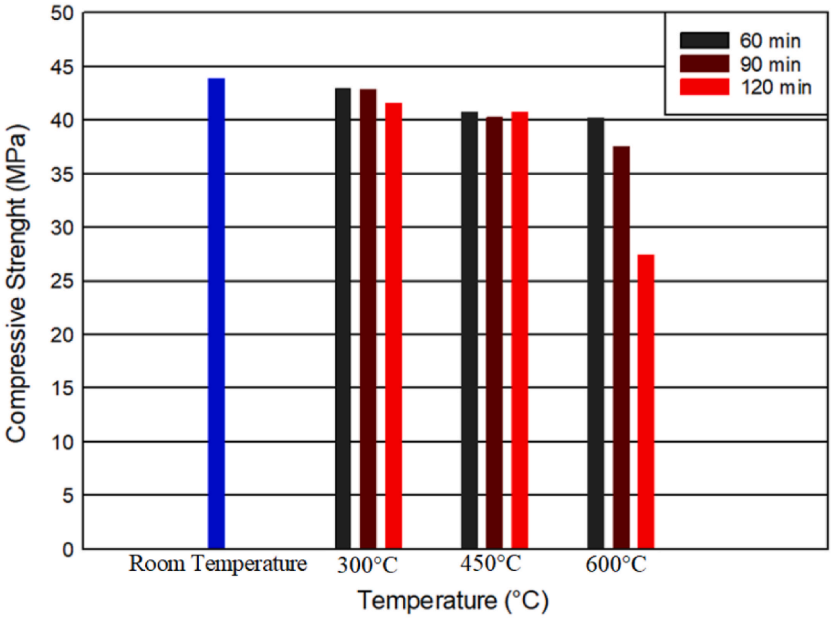

Fig. 5. Graphical depiction of data from concrete samples that are UNP.

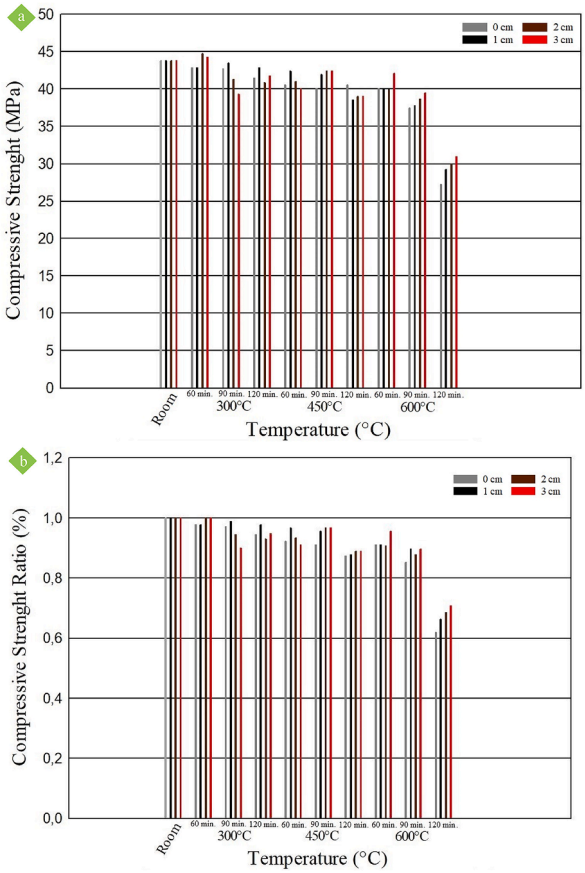

Fig. 6. a. Representation of the CSs for samples with CIP at thicknesses of 0, 1, 2, and 3 cm, recorded at both room temperature and elevated temperatures of 300, 450, and 600 °C, b. CS rates.

thickness and exposed to a temperature of 300 °C, the reduction in CS does not exhibit a linear correlation with the plaster thickness. As a result, the data collected at this temperature does not allow for the formulation of a definitive conclusion. After the concrete specimens are subjected to a temperature of 450 °C, the CIP effectively prevents the decline in CS in the samples exposed for 90 and 120-min. Specifically, when the CIP thickness is 3 cm, there is a notable 7% reduction in the reduction of concrete CS at 450 °C when compared to UNP concrete. If it is focused on the column block at 600 °C with a 120-min exposure time, the strength of the 0 cm thick sample is 27.44 MPa, while the 3 cm thick CIP sample shows a strength of 31.19 MPa. This observation highlights an improvement of approximately 14% in the CS of the 3 cm thick CIP sample compared to the standard concrete sample without plaster under the same conditions of 600 °C and 120-min of exposure.

The graph presented in Fig. 6b is created by dividing the CS values obtained after exposure to high temperatures at their specific thicknesses by the CS values obtained at room temperature for each sample. The results from this graph indicate that when the models are insulated with CIP, there is a more minor 8% reduction in their CS compared to the UNP samples. Moreover, examining the reductions in concrete CS in Fig. 6b reveals the tangible influence of CIP on safeguarding concrete in samples suffered from temperatures exceeding 450 °C for longer than 60-min.

The samples depicted in Fig. 7 exemplify both UNP and plastered concrete specimens subjected to a 60-min exposure at 450 °C. As illustrated in the figure, there is an observable alteration in colour for the samples exposed to this temperature, along with minor spillage on the plastered surfaces. Nonetheless, it is noteworthy that the anticipated spillage does not occur in cases where RP or CIP is applied. It is pretty evident that the CIP provides comprehensive safeguarding against unforeseen events such as high-temperature fires.

Fig. 8a displays the CSs of RP concrete at various thicknesses (0, 1, 2, and 3 cm) under different conditions: room temperature and elevated temperatures of 300 °C, 450 °C, and 600 °C for durations of 60, 90, and 120-min. It also includes the average CSs of concretes maintained at room temperature for reference. In Fig. 8b–a noticeable trend emerges where the CS of concrete decreases when exposed to higher temperatures. For instance, at room temperature, the average CS is 43,895 MPa, but when subjected to 600 °C for 120-min, this value drops to around 28.045 MPa. On the other hand, the CS values extracted from the samples following 60-min and 90-min of exposure are gauged at 41.985 MPa and 37.67 MPa, correspondingly. In conclusion, based on the CS test data derived from the sample at room temperature, there is a decline of roughly 4.35%, 14.2%, and 36.1% in the data acquired after 60, 90, and 120-min of exposure, severally. Therefore, this effect is approximately eight times more pronounced for the samples coated with regular plaster. Furthermore, Fig. 8b presents CS ratios obtained by dividing the CS of concrete exposed to elevated temperatures by the CS of samples kept at room temperature. RP serves as a protective barrier, preventing direct exposure of the concrete surface to high temperatures, consequently minimising damage to the concrete. It is self-evident that RP is relatively effective in preserving the structural integrity of concrete under high-temperature conditions. Concrete exposed to 600 °C for 120-min, for instance, exhibits an approximate 2.2% protective effect on the CS of RP concrete.

Fig. 7. Samples, both with and without plaster, which is exposed to a temperature of 450 °C for 60-min.

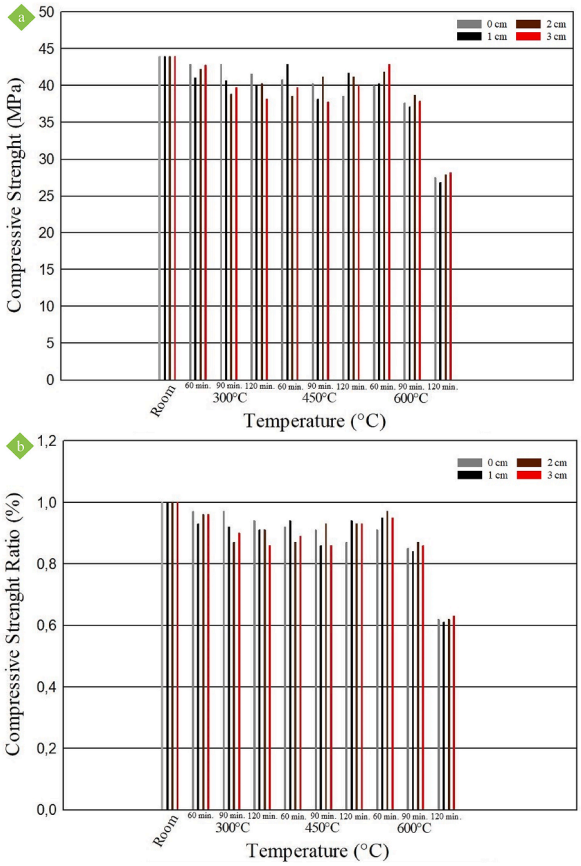

Fig. 8. a. CSs of UNP, 1.2 and 3 cm thick RP concrete at room temperature and 300 °C, 450 °C and 600 °C, b. CS rates.

In Fig. 9a, the graphic displays the CS results for different types of samples, including UNP, CIP, and RP samples. These samples are exposed to the highest temperature (600 °C) utilised in the experimental study for durations of 60, 90, and 120-min. The purpose of the graph is to effectively illustrate the effectiveness of the study in terms of CS values. Each of the plastered samples possesses thicknesses of 1, 2, and 3 cm, and multiple samples are prepared for each consistency. The presented values represent the averages of the results obtained from these various samples. As depicted in the graph, there is a noticeable reduction in CS due to the degradation of the internal structure of the structures when subjected to elevated temperatures. This reduction is directly related to both the duration of exposure and the temperature level. Additionally, the graph illustrates that increasing the thickness of plaster applications on the samples results in improvements in mitigating CS losses. However, it is evident from the graph that the CIP significantly outperforms other application methods in terms of its effectiveness. On the contrary, Fig. 9b presents a chart derived from dividing the CS values obtained from samples with CIP and RP exposed to 600 °C for 60, 90, and 120-min by the CS value measured at room temperature. When examining the ratios of concrete CS, it becomes evident that the plastered samples experience less reduction in CS compared to the UNP ones. This indicates that applying plaster to structures acts as a protective measure against sudden high-temperature conditions. During the experiment, the protective effect of plastered concrete under high temperatures is most recognisable in samples subjected to a 120-min exposure. Consequently, the CS ratio for RP samples compared to UNP ones improves by more than 2%. In contrast, this ratio is 6% for samples with CIP compared to UNP, and it increases to over 14% for samples with a 3 cm thickness of CIP. Furthermore, it is apparent that insulation-plastered concrete samples have a 7% lower CS loss compared to UNP models, providing a 5% advantage over RP concrete samples.

3.1. Thermophysical behaviour of the sample under elevated temperature

3.1.1. SEM analysis

Microscopic images captured from the sample in Fig. 10a reveal the internal structure magnified 10,000 times. Depicting the product formed by the interaction of perlite and water, precisely the lime reaction, the picture emphasises needle-like structures with diverse views of their internal arrangement. The purpose is to prove the integrity of these structures visually. However, whilst Fig. 10b, which presents the image of the sample exposed to 300 °C, shows signs of small cracks forming in certain parts of the expanded perlite, Fig. 10c indicates that these cracks widen when the temperature reaches 450 °C. On the other hand, Fig. 10d observes the internal structure of the sample when it arrives at 600 °C, five times closer than Fig. 10c. Accordingly, on looking at its internal structure, the cracks that appear exhibit that most of the bonds formed because of the reaction have been broken. In contrast, when approached

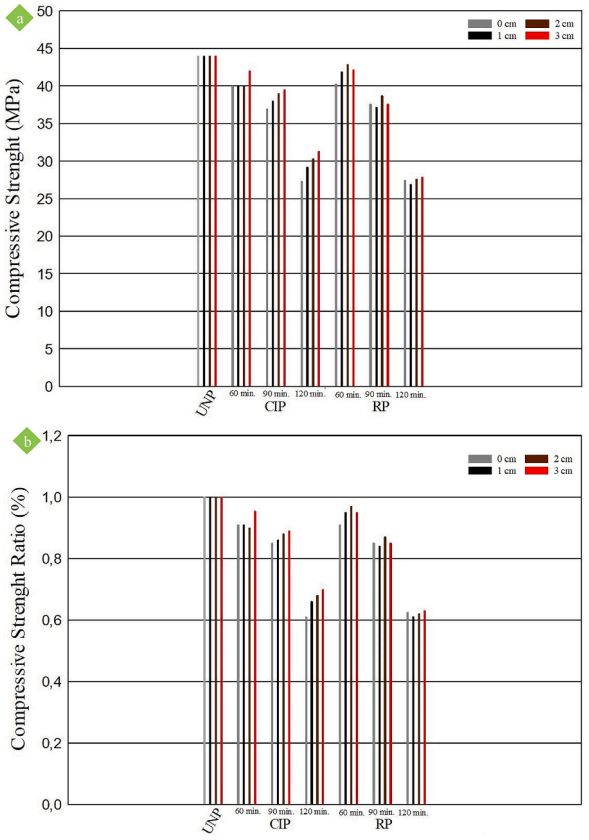

Fig. 9. a. Graph of the CS resulting from exposing UNP, CIP, and RP samples at 600 °C for different durations, b. CS rates.

further, it can be easily seen that it is accompanied by small-scale fractures in the body structure. It can also be interpreted that the increment in cracks occurring in the sample at 600 °C is due to the release of CO_2, and therefore, the interconnections in the structure are broken. Consequently, this gives rise to mechanical cracks and a subsequent reduction in strength and sensitivity.

3.1.2. Thermogravimetric analysis

In the experimental study, a piece from the sample is subjected to TGA. The results of this analysis reveal that as the temperature of the sample increases to 100 °C, the moisture within it begins to evaporate. Subsequently, the polymer fibre gradually diminishes from the sample, keeping doing so until reaching approximately 650 °C. In the temperature range of 680–740 °C, carbon dioxide (CO_2) is released from the calcite ($CaCO_3$) contained in the sample. Consequently, the structure remaining within the model transforms into lime (CaO) instead of $CaCO_3$. These values and interpretations are derived from the data presented in Fig. 11.

3.1.3. X-ray diffraction analysis

The XRD analysis method is employed to determine the mineralogical distribution of powder samples collected both before and after exposure to elevated temperatures. Utilising the PW1830 model device with λCu-K-beta wavelengths, the powder samples underwent scanning within the 4°-90°-2θ°. Fig. 12 displays the XRD textures graph. The Qualx program defines the mineralogical composition of the primary reaction phases [34–36]. In the analysis, pre-heat plaster mortar powders are denoted as 1, whilst post-heat plaster mortar powders are marked as 2. The dominant reaction phases before the temperature rise are identified as Quartz (40.23, 45.73, 50.08, 54.80, 63.96, 73.40) and Calcite (31.43, 39.40, 47.11, 57.39, 65.61, 83.76). Upon scrutinising the graph, a texture exhibiting high crystallinity and a low amorphous phase structure is evident before heating. Subsequent to the temperature increase, the XRD analysis reveals the disappearance of Quartz peaks and a shift in Calcite peaks (29.35, 35.89, 47.13, 57.49, 61.36). This indicates a degradation in the crystalline structure post-temperature application, transitioning into a more amorphous, dispersed, and irregular structure, impacting the material's strengths. The compromised internal structure is observed to induce alterations in the gel structure of the plaster mortars. Additionally, the XRD graph post-temperature exhibits narrowed peak depth and width, signifying a shift from a crystalline to an amorphous structure.

4. Regression analysis

After conducting practical experiments using existing data, regression analysis is employed to forecast the behaviour of a system or phenomenon under future extreme conditions that are not specifically studied. This forecast is made using the variables identified

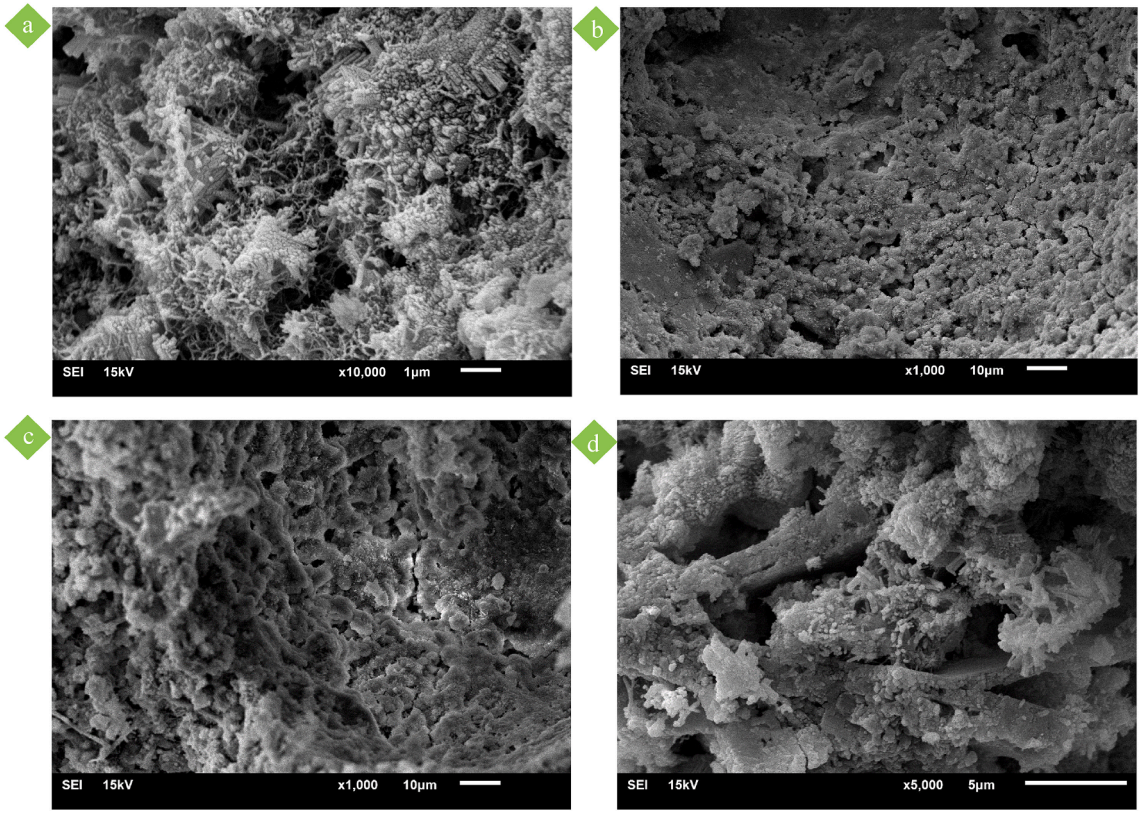

Fig. 10. a. A microscope's scanning electron microscope (SEM) image of the sample at normal room temperature, b. 300 °C, c. 450 °C, d. 600 °C.

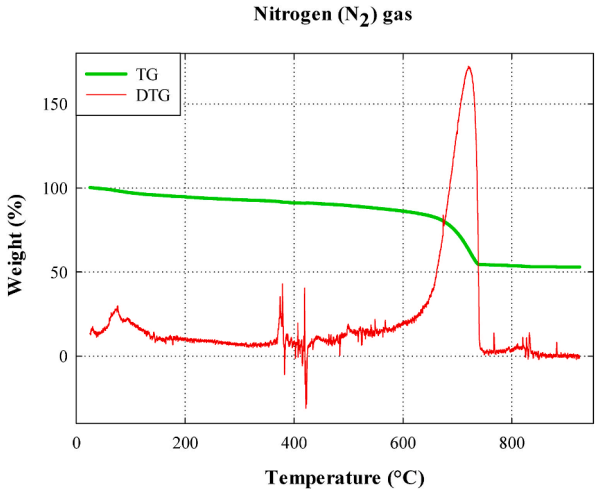

Fig. 11. Analysis of the sample used in the experiment through thermogravimetric analysis (TGA).

and analysed during the initial stage of the study. In this work, SigmaPlot 15.0 is utilised for running the regression analysis, emphasising assessing fire resistance, where a thickness of 2 cm is projected to be adequate. The data used in the regression analysis is written in Tables 3 and 4.

The initial step in applying regression analysis involves selecting the equation with the highest predictive accuracy, signifying the most precise curve fit based on the data graph. In this study, it is observed that the most suitable equation is derived from the Logarithm - 2nd Order equation. As the temperature continues to increase and there is a rapid course of changes in the internal structure of the sample, which remains in a constantly closed furnace environment, it is concluded that it is appropriate to prefer logarithmic in this regression study. In addition, Chen et al. [37], who conduct a similar study, added a temperature-CS graph to the fibre-reinforced concrete sample using a different model, and it is seen that it possesses a similar trend to our research. In addition to this, the selection

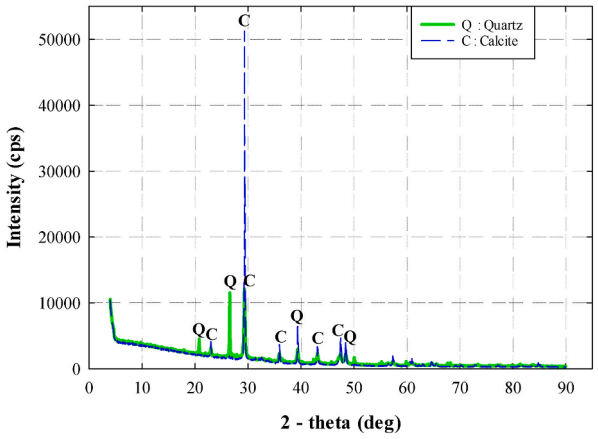

Fig. 12. Graphical representation obtained from x-ray diffraction (XRD) analysis of a sample with Quartz and Calcite constituting its internal structure.

Table 3
Temperature and corresponding CS data for a 2 cm thick CIP sample at 120-min analysed in this context.

Temperature, °C	CS, MPa
300	40.985
450	39.23
600	30.28

Table 4
Time and corresponding CS data for a 2 cm thick CIP sample at 600 °C analysed in this context.

Time, min	CS, MPa
60	39.9
90	38.855
120	30.28

of the most appropriate equation is determined by evaluating the coefficient of determination, denoted as the R^2 value. The R^2 value ranges from 0 to 1, with 0 indicating a poor fit and 1 signifying a perfect curve fit. The equation sets in this analysis confirm that an almost ideal curve fit is achieved with an R^2 value of 0.996. Consequently, the primary objective is to derive the equation based on the values of the 2 cm thick CIP sample with a 120-min exposure time and predict the temperature at which the CS value reaches 10 MPa. Besides, the second objective is to formulate an equation by utilising the CS values of a given sample at 600 °C over various time intervals and to calculate the time it takes for the CS value to reach 10 MPa. Following the curve fitting procedure in SigmaPlot, equation 1 through 3 are generated, and the most appropriate equation is displayed. Subsequently, the forecasted result is documented after performing the required operations on these equations.

$$F_{CS} = y_0 + a\ \ln\ T + b(\ln\ T)^2 \tag{1}$$

$$y_0 = -1280.7273, a = 452.1129, b = -38.6388 \tag{2}$$

When the collected data is input into the equation and refined, it takes the form of Equation (3).

$$F_{CS} = -38.6388(\ln\ T)^2 + 452.1129\ \ln\ T - 1280.7273 \tag{3}$$

To restore the equation to its familiar form, it can be simplified by substituting a variable, like “u” for “ln T”.

$$F_{CS} = -38.6388u^2 + 452.1129u - 1280.7273 = 10 \tag{4}$$

$$-38.6388u^2 + 452.1129u - 1290.7273 = 0 \tag{5}$$

$$c = -38.6388, d = 452.1129, e = -1290.7273 \tag{6}$$

$$\sqrt{\Delta} = \sqrt{d^2 - 4ce} = \sqrt{(452.1129)^2 - 4 \times (-38.6388) \times (-1290.7273)} \cong 70.125 \tag{7}$$

$$y_{1,2} = \frac{-d \pm \sqrt{\Delta}}{2c}, y_1 \cong 4.94, y_2 \cong 6.76 \tag{8}$$

$$y_1 = \log_e T_1 \rightarrow T_1 = 139.78°C \; y_2 = \log_e T_2 \rightarrow T_2 \cong 861°C \tag{9}$$

Based on the findings, the most accurate temperature estimate is approximately 861 °C.

On the other hand, similar procedures are attempted to estimate the time at the specified temperature using the data in Table 4. Accordingly, the formula used in this context remains consistent, and the unknown parameters with this dataset are as follows.

$$y_0 = -673.3159, a = 335.0395, b = -39.2845 \tag{10}$$

Likewise, when the gathered data is logged into the equation and undergoes refinement, it transforms into Equation (4).

$$F_{CS} = -39.2845\left(\ln\ t_{exp}\right)^2 + 335.0395\ \ln\ t_{exp} - 673.3159 \tag{11}$$

In order to bring the equation back to its recognisable format, it can be made more straightforward by replacing a variable, such as "u", in place of "ln t_{exp}". Following some intermediate computations, the estimated time is roughly 173-min. Fig. 13a and b depict the graphic representation linked to these predictions.

5. CFD analysis for verification

A computational fluid dynamics (CFD) analysis is acted to emphasise the significance of the CIP utilised in this experimental investigation. To achieve this goal, in the initial phase, geometric models are constructed for samples coated with UNP, CIP, and RP using Fluent-based CFD simulations, following the dimensions applied in the experimental study. These dimensions correspond to UNP, 1-1 RP, 1-1 CIP, and 2-2 CIP, respectively. Subsequently, the default mesh is used for the samples. This sample is described as entirely perfectly insulated for edge surfaces as well as also its top and bottom, designated as hot and cold, individually. After performing the necessary fluid-related operations, the results indicate that the CIP accumulates in a specific region of the hot surface. Furthermore, as it progresses inward, its heat resistance becomes evident in Fig. 14 when compared to the other RP and UNP samples.

6. Conclusion

This research sheds light on the resilience of CIP structures when exposed to severe conditions at elevated temperatures, particularly without plaster or with RP surfaces. In the study, RP and CIP are applied to the surface of each sample at thicknesses of 1 cm, 2 cm, and 3 cm. Subsequently, the samples are subjected to oven temperatures of 300 °C, 450 °C, and 600 °C for 60, 90, and 120-min durations. Afterwards, the plasters are removed from the samples, and the CS test is performed. The findings from this experimental investigation are outlined as follows.

- The study has revealed that the CIP employed in this research offers significant protection against potential fires that might occur in residential or commercial settings.
- In contrast to the typical fibre structures commonly discussed in the literature, the study's primary focus, CIP, demonstrates significantly superior effectiveness.
- It appears that the dimensions of concrete samples have an impact on their resistance. Specifically, as the size increases, the influence of the fire becomes more pronounced.
- An increment in plaster thickness corresponds to an enhancement in thermal resistance against fire.
- Based on the experimental findings, the CS of UNP samples, which is 43.9 MPa at room temperature, decreases to 27.435 MPa when exposed to 600 °C for 120-min. This represents a reduction of approximately 37.5%.
- The experimental findings reveal that, when subjected to the same extreme conditions, the 3 cm thick CIP-coated sample attains a value of 31.19 MPa, which remains above the 30 MPa threshold. This signifies a reduction of roughly 28.95% when compared to the value recorded at room temperature.

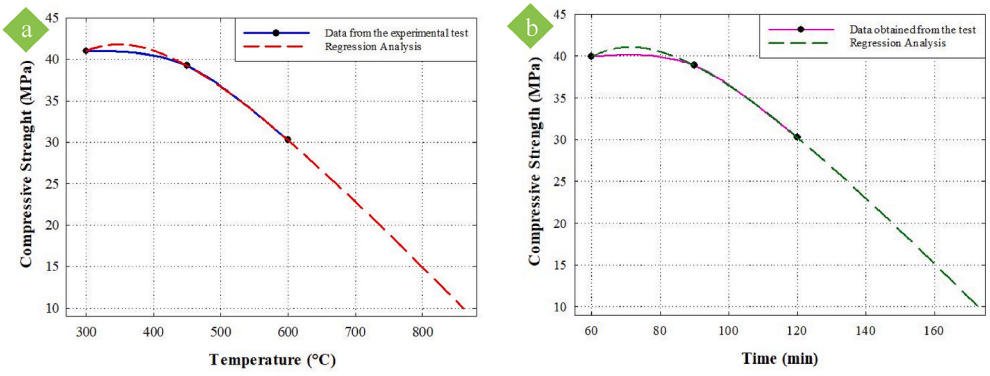

Fig. 13. a. Graph illustrating the relationship between temperature and CS based on experimental test data and regression analysis results, b. Graph depicting the correlation between time and CS derived from experimental test data and regression analysis outcomes.

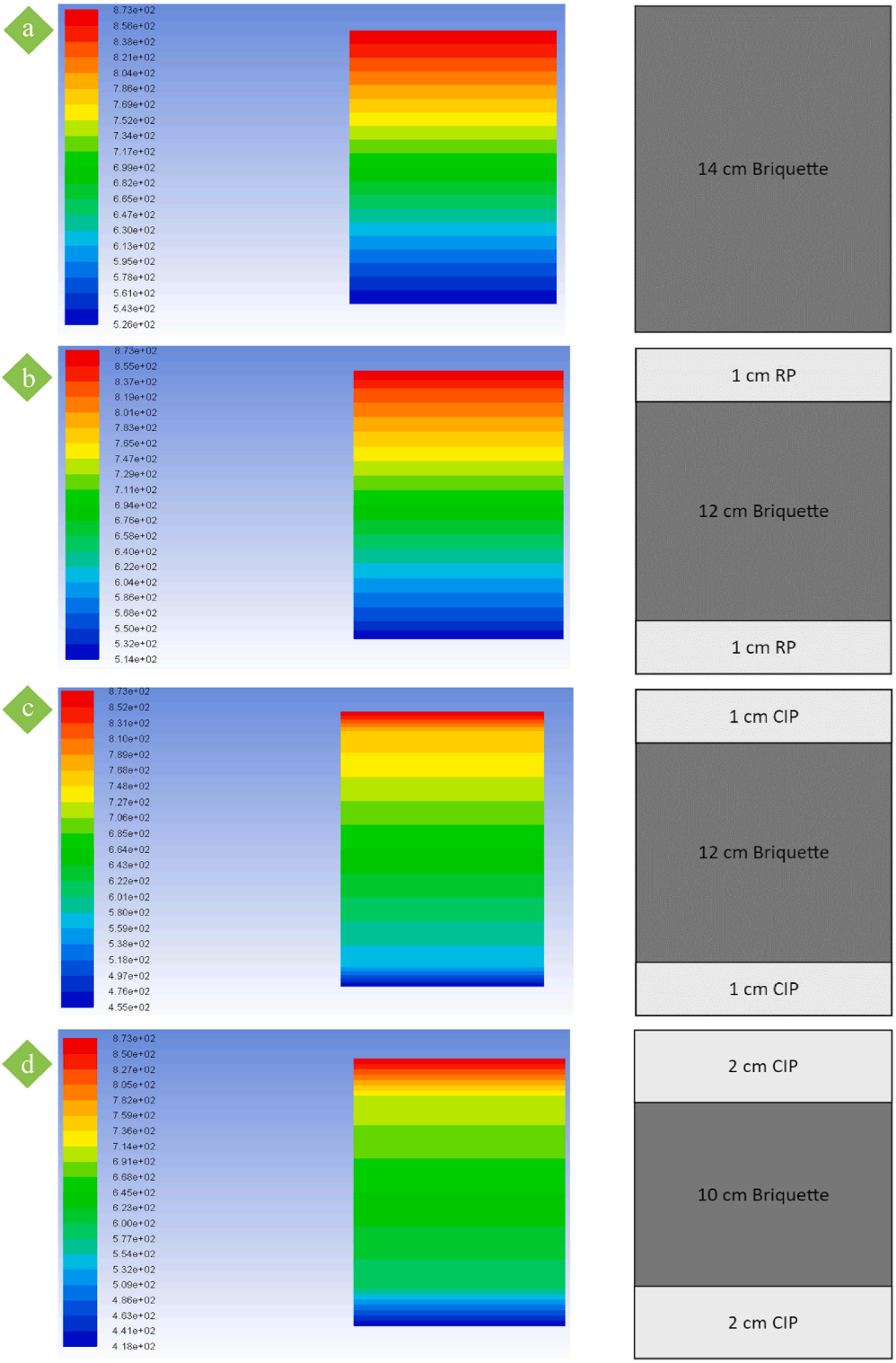

Fig. 14. a. Examination of the thermal performance of UNP briquettes at elevated temperatures, b. 1-1 RP, c. 1-1 CIP, d. 2-2 CIP.

- Under identical conditions, the 3 cm thick RP sample exhibits a value of 28.045 MPa. In this scenario, there is a reduction of 36.11% compared to the initial value at room temperature.
- Clearly, CIP demonstrates a 13.4% superior performance compared to RP, which already contributes to relatively favourable outcomes.

- Based on the results acquired from the XRD analysis, it has been visually demonstrated that the decline in hardness strength is a consequence of the degradation of the Quartz structure in samples exposed to elevated temperatures.
- In the context of regression analysis, the optimal probability value for curve formation (R^2) is 0.996. Besides, when determining the temperature range within which the value of 10 MPa will occur for a duration of 120-min, using a 2 cm CIP sample, the outcome indicates that it is around 861 °C.
- When assessing the time needed to lower the pressure of another sample possessing the same characteristics as previously described to 10 MPa at 600 °C, the outcome indicates an approximate duration of 173-min.
- To enhance comprehension of the distinctions between the CIP, RP, and UNP utilised in the experiment, validation is performed through CFD analysis. Visual representations unequivocally reveal that the temperature within the CIP-covered area is contained within that region, leading to a reduction in the temperature infiltrating the briquette.

CRediT authorship contribution statement

Ilker Ustabas: Methodology, Conceptualization. **Pinar Mert Cuce:** Conceptualization, Formal analysis, Writing – original draft. **Emre Alvur:** Software, Formal analysis. **Duygu Kesepara:** Formal analysis, Investigation. **Yusuf Nadir Yilmaz:** Formal analysis, Software. **Erdem Cuce:** Writing – review & editing, Supervision, Methodology, Investigation, Conceptualization. **Saad Alshahrani:** Funding acquisition, Writing – review & editing.

Declaration of competing interest

The authors declare no conflict of interest.

Data availability

No data was used for the research described in the article.

Acknowledgment

The authors extend their appreciation to the Deanship of Scientific Research at King Khalid University for funding this work through a large group project under grant number RGP2/106/44.

References

[1] A.M. Rashad, Possibility of using metakaolin as thermal insulation material, Int. J. Thermophys. 38 (2017) 1–11.
[2] C.S. Poon, S. Azhar, M. Anson, Y.L. Wong, Strength and durability recovery of fire-damaged concrete after post-fire-curing, Cement Concr. Res. 31 (9) (2001) 1307–1318.
[3] G.A. Khoury, Effect of fire on concrete and concrete structures, Prog. Struct. Eng. Mater. 2 (4) (2000) 429–447.
[4] U. Schneider, Concrete at high temperatures—a general review, Fire Saf. J. 13 (1) (1988) 55–68.
[5] B.M. Luccioni, M.I. Figueroa, R.F. Danesi, Thermo-mechanic model for concrete exposed to elevated temperatures, Eng. Struct. 25 (6) (2003) 729–742.
[6] G.A. Khoury, C.E. Majorana, F. Pesavento, B.A. Schrefler, Modelling of heated concrete, Mag. Concr. Res. 54 (2) (2002) 77–101.
[7] G.A. Khoury, Effect of fire on concrete and concrete structures, Prog. Struct. Eng. Mater. 2 (4) (2000) 429–447.
[8] T. Ayub, N. Shafiq, S.U. Khan, M. Nuruddin, Durability of concrete with different mineral admixtures: a review, International Journal of Civil, Architectural, Structural and Construction Engineering 7 (8) (2013) 273–284.
[9] C.S. Poon, S. Azhar, Deterioration and recovery of metakaolin blended concrete subjected to high temperature, Fire Technol. 39 (2003) 35–45.
[10] M. Heikal, Effect of temperature on the structure and strength properties of cement pastes containing fly ash alone or in combination with limestone, Ceramics 50 (3) (2006) 167.
[11] D. Qin, P. Gao, F. Aslam, M. Sufian, H. Alabduljabbar, A comprehensive review on fire damage assessment of reinforced concrete structures, Case Stud. Constr. Mater. 16 (2022) e00843.
[12] T. Kiran, S.K. Yadav, N. Anand, M.E. Mathews, D. Andrushia, V. Kodur, Performance evaluation of lightweight insulating plaster for enhancing the fire endurance of high strength structural concrete, J. Build. Eng. 57 (2022) 104902.
[13] J.H. Lee, Y.S. Sohn, S.H. Lee, Fire resistance of hybrid fibre-reinforced, ultra-high-strength concrete columns with compressive strength from 120 to 200 MPa, Mag. Concr. Res. 64 (6) (2012) 539–550.
[14] M. Asamatdinov, A. Zhukov, A. Medvedev, V. Mukhametzyanov, Fire protection systems using clay-gypsum plaster in agriculture, E3S Web of conferences 175 (2020), 11008 EDP Sciences.
[15] Q. Li, J. Yao, T. Liang, Experimental study on the effect of fireproof coating and cooling methods on the mechanical properties of concrete exposed to high temperature, Construct. Build. Mater. 376 (2023) 131045.
[16] S. Aydın, B. Baradan, Effect of pumice and fly ash incorporation on high temperature resistance of cement based mortars, Cement Concr. Res. 37 (6) (2007) 988–995.
[17] T. Kiran, N. Anand, A.D. Andrushia, V. Kodur, M.E. Mathews, G.P. Arulraj, Performance of clay masonry prisms with light weight plaster exposed to standard fire exposure, Fire Mater. 47 (1) (2023) 99–119.
[18] M. Zulkifeli, H.B. Saman Mohamed, Compressive and flexural strength of expanded perlite aggregate mortar subjected to high temperatures, in: AIP Conference Proceedings. August, 2017, p. 1875 1.
[19] S. Aydın, Development of a high-temperature-resistant mortar by using slag and pumice, Fire Saf. J. 43 (8) (2008) 610–617.
[20] F. Koksal, K. Coşar, M. Dener, A. Benli, O. Gencel, Insulating and fire-resistance performance of calcium aluminate cement based lightweight mortars, Construct. Build. Mater. 362 (2023) 129759.
[21] G. Ma, K. Jia, P. Xie, A. Ruhan, L. Wang, X. Ding, D. Ju, Physical, mineralogical, thermal, and mechanical properties of aerogel-incorporated concrete exposed to elevated temperatures, Cement Concr. Compos. 140 (2023) 105089.
[22] M. Li, C. Qian, W. Sun, Mechanical properties of high-strength concrete after fire, Cement Concr. Res. 34 (6) (2004) 1001–1005.
[23] D.N. Bilow, M.E. Kamara, Fire and concrete structures, in: Proceedings of the ASCE Structures Congress 2008: Crossing Borders, Vancouver, Canada, 2008, p. 10.
[24] A. Alaskar, A. Albidah, A.S. Alqarni, R. Alyousef, H. Mohammadhosseini, Performance evaluation of high-strength concrete reinforced with basalt fibers exposed to elevated temperatures, J. Build. Eng. 35 (2021) 102108.
[25] D.H. Reddy, A. Ramaswamy, Influence of mineral admixtures and aggregates on properties of different concretes under high temperature conditions I: experimental study, J. Build. Eng. 14 (2017) 103–114.

[26] T.G.G. Molay, M.N.L. Leroy, T. Fidele, H.G. Franck, N.J.M. Bienvenu, Mechanical and physical performances of concretes made from crushed sands of different geological nature subjected to high temperatures, Engineering Science and Technology, an International Journal 22 (4) (2019) 1116–1124.
[27] J. Shen, Q. Xu, Effect of elevated temperatures on compressive strength of concrete, Construct. Build. Mater. 229 (2019) 116846.
[28] A.R. Mundhada, A.D. Pofale, Effect of high temperature on compressive strength of concrete, IOSR J. Mech. Civ. Eng. 12 (1) (2015) 66–70.
[29] E. Sancak, Y.D. Sari, O. Simsek, Effects of elevated temperature on compressive strength and weight loss of the light-weight concrete with silica fume and superplasticizer, Cement Concr. Compos. 30 (8) (2008) 715–721.
[30] E. Cuce, P.M. Cuce, E. Alvur, Y.N. Yilmaz, S. Saboor, I. Ustabas, E. Linul, M. Asif, Experimental performance assessment of a novel insulation plaster as an energy-efficient retrofit solution for external walls: a key building material towards low/zero carbon buildings, Case Stud. Therm. Eng. 49 (2023) 103350.
[31] R. Jack, D. Loveday, D. Allinson, K. Lomas, First evidence for the reliability of building co-heating tests, Build. Res. Inf. 46 (4) (2018) 383–401.
[32] D. Johnston, D. Miles-Shenton, D. Farmer, J. Wingfield, Whole House Heat Loss Test Method (Coheating), Leeds Metropolitan University, Leeds, UK, 2013.
[33] D. Johnston, J. Wingfield, D. Miles-Shenton, Measuring the fabric performance of UK dwellings, in: Proceedings of the Association of Researchers in Construction Management (ARCOM) Twenty-Sixth Annual Conference, vol. 2, 2010, pp. 1371–1380.
[34] Z. Kurt, İ. Ustabaş, T. Cakmak, Novel binder material in geopolymer mortar production: obsidian stone powder, Struct. Concr. 24 (4) (2023) 5600–5613.
[35] A. Bouaissi, L.Y. Li, M.M.A.B. Abdullah, Q.B. Bui, Mechanical properties and microstructure analysis of FA-GGBS-HMNS based geopolymer concrete, Construct. Build. Mater. 210 (2019) 198–209.
[36] I.H. Aziz, M.M.A.B. Abdullah, M.M. Salleh, E.A. Azimi, J. Chaiprapa, A.V. Sandu, Strength development of solely ground granulated blast furnace slag geopolymers, Construct. Build. Mater. 250 (2020) 118720.
[37] H. Chen, J. Yang, X. Chen, A convolution-based deep learning approach for estimating compressive strength of fiber reinforced concrete at elevated temperatures, Construct. Build. Mater. 313 (2021) 125437.